Research Article
Vol. 25, No. 19 | 18 Sep 2017 | OPTICS EXPRESS 22710
Optics EXPRESS

Fluid jet-array parallel machining of optical microstructure array surfaces

CHUNJIN WANG, CHI FAI CHEUNG,* MINGYU LIU, AND WING BUN LEE

Partner State Key Laboratory of Ultra-precision Machining Technology, Department of Industrial and Systems Engineering, The Hong Kong Polytechnic University, Hung Hom, Kowloon, Hong Kong
** Benny.Cheung@polyu.edu.hk*

Abstract: Optical microstructure array surfaces such as micro-lens array surface, micro-groove array surface etc., are being used in more and more optical products, depending on its ability to produce a unique or particular performance. The geometrical complexity of the optical microstructures array surfaces makes them difficult to be fabricated. In this paper, a novel method named fluid jet-array parallel machining (FJAPM) is proposed to provide a new way to generate the microstructure array surfaces with high productivity. In this process, an array of abrasive water jets is pumped out of a nozzle, and each fluid jet simultaneously impinges the target surface to implement material removal independently. The jet-array nozzle was optimally designed firstly to diminish the effect of jet interference based on the experimental investigation on the 2-Jet nozzles with different jet intervals. The material removal and surface generation models were built and validated through the comparison of simulation and experimental results of the generation of several kinds of microstructure array surfaces. Following that, the effect of some factors in the process was discussed, including the fluid pressure, nozzle geometry, tool path, and dwell time. The experimental results and analysis prove that FJAPM process is an effective way to fabricate the optical microstructure array surface together with high productivity.

OCIS codes: (220.5450) Polishing; (220.4000) Microstructure fabrication; (120.4610) Optical fabrication.

References and links

1. L. Li and A. Y. Yi, "Development of a 3D artificial compound eye," Opt. Express **18**(17), 18125–18137 (2010).
2. L. B. Kong, C. F. Cheung, X. Q. Jiang, W. B. Lee, S. To, L. Blunt, and P. Scott, "Characterization of surface generation of optical microstructures using a pattern and feature parametric analysis method," Precis. Eng. **34**(4), 755–766 (2010).
3. D. Xu, J. D. Owen, J. C. Papa, J. Reimers, T. J. Suleski, J. R. Troutman, M. A. Davies, K. P. Thompson, and J. P. Rolland, "Design, fabrication, and testing of convex reflective diffraction gratings," Opt. Express **25**(13), 15252–15268 (2017).
4. M. Mao and J. W. Yan, "Ductile machining of single-crystal silicon for microlens arrays by ultraprecision diamond turning using a slow tool servo," Int. J. Mach. Tools Manuf. **115**, 2–14 (2017).
5. Y. H. Ko and J. S. Yu, "Highly transparent sapphire micro-grating structures with large diffuse light scattering," Opt. Express **19**(16), 15574–15583 (2011).
6. X. H. Lee, I. Moreno, and C.-C. Sun, "High-performance LED street lighting using microlens arrays," Opt. Express **21**(9), 10612–10621 (2013).
7. T. Hou, C. Zheng, S. Bai, Q. Ma, D. Bridges, A. Hu, and W. W. Duley, "Fabrication, characterization, and applications of microlenses," Appl. Opt. **54**(24), 7366–7376 (2015).
8. C. Florian, S. Piazza, A. Diaspro, P. Serra, and M. Duocastella, "Direct laser printing of tailored polymeric microlenses," ACS Appl. Mater. Interfaces **8**(27), 17028–17032 (2016).
9. H. Lin, J. Gao, Q. Mei, Y. He, J. Liu, and X. Wang, "Adaptive digital fringe projection technique for high dynamic range three-dimensional shape measurement," Opt. Express **24**(7), 7703–7718 (2016).
10. Z. Cai, X. Liu, X. Peng, Y. Yin, A. Li, J. Wu, and B. Z. Gao, "Structured light field 3D imaging," Opt. Express **24**(18), 20324–20334 (2016).
11. Y. Caulier, "Inspection of complex surfaces by means of structured light patterns," Opt. Express **18**(7), 6642–6660 (2010).
12. C. D. Torres, P. J. Heaney, A. V. Sumant, M. A. Hamilton, R. W. Carpick, and F. E. Pfefferkorn, "Analyzing the performance of diamond-coated micro end mills," Int. J. Mach. Tools Manuf. **49**(7), 599–612 (2009).
13. C. Iliescu, B. Chen, and J. Miao, "On the wet etching of Pyrex glass," Sens. Actuators A Phys. **143**(1), 154–161 (2008).

#301815
https://doi.org/10.1364/OE.25.022710
Journal © 2017
Received 5 Jul 2017; revised 26 Aug 2017; accepted 4 Sep 2017; published 8 Sep 2017
Corrected: 11 September 2017

14. G. Cusanelli, A. Hessler-Wyser, F. Bobard, R. Demellayer, R. Perez, and R. Flükiger, "Microstructure at submicron scale of the white layer produced by EDM technique," J. Mater. Process. Technol. **149**(1), 289–295 (2004).
15. B. McCall and T. S. Tkaczyk, "Rapid fabrication of miniature lens arrays by four-axis single point diamond machining," Opt. Express **21**(3), 3557–3572 (2013).
16. H. Zhang, L. Li, D. L. McCray, S. Scheiding, N. J. Naples, A. Gebhardt, S. Risse, R. Eberhardt, A. Tünnermann, and A. Y. Yi, "Development of a low cost high precision three-layer 3D artificial compound eye," Opt. Express **21**(19), 22232–22245 (2013).
17. Z. Zhu, S. To, and S. Zhang, "Large-scale fabrication of micro-lens array by novel end-fly-cutting-servo diamond machining," Opt. Express **23**(16), 20593–20604 (2015).
18. J. Li, F. Zhao, and W. C. Shih, "Direct-write patterning of nanoporous gold microstructures by in situ laser-assisted dealloying," Opt. Express **24**(20), 23610–23617 (2016).
19. I. Saxena, K. Ehmann, and J. Cao, "High throughput microfabrication using laser induced plasma in saline aqueous medium," J. Mater. Process. Technol. **217**, 77–87 (2015).
20. X. Cheng, Z. Wang, K. Nakamoto, and K. Yamazaki, "A study on the micro tooling for micro/nano milling," Int. J. Adv. Manuf. Technol. **53**(5–8), 523–533 (2011).
21. O. Iordan and C. Burlacu, "The main factors of influence in the micro-milling field," Academic J. Manuf. Eng. **48**, 43–49 (2010).
22. C.-Y. Huang, C.-H. Kuo, W.-T. Hsiao, K.-C. Huang, S.-F. Tseng, and C.-P. Chou, "Glass biochip fabrication by laser micromachining and glass-molding process," J. Mater. Process. Technol. **212**(3), 633–639 (2012).
23. G. Kucukturk and C. Cogun, "A new method for machining of electrically nonconductive workpieces using electric discharge machining technique," Mach. Sci. Technol. **14**(2), 189–207 (2010).
24. H. Ogura and Y. Yoshida, "Hole drilling of glass substrates with a CO2 laser," Jpn. J. Appl. Phys. **42**(5), 2881–2886 (2003).
25. J. Yang, F. Luo, T. S. Kao, X. Li, G. W. Ho, J. Teng, X. Luo, and M. Hong, "Design and fabrication of broadband ultralow reflectivity black Si surfaces by laser micro/nanoprocessing," Light Sci. Appl. **3**(7), e185 (2014).
26. D. A. Axint, B. Karpuschewski, M. C. Kong, A. T. Beaucamp, S. Anwar, D. Miller, and M. Petzel, "High energy fluid jet machining (HEFJet-Mach): from scientific and technological advances to niche industrial applications," CIRP Annals-Manuf. Technol. **63**(2), 751–771 (2014).
27. N. Haghbin, J. K. Spelt, and M. Papini, "Abrasive waterjet micro-machining of channels in metals: Model to predict high aspect-ratio channel profiles for submerged and unsubmerged machining," J. Mater. Process. Technol. **222**, 399–409 (2015).
28. N. Haghbin, J. K. Spelt, and M. Papini, "Abrasive waterjet micro-machining of channels in metals: comparison between machining in air and submerged in water," Int. J. Mach. Tools Manuf. **88**, 108–117 (2015).
29. O. W. Fähnle, H. Brug, and H. J. Frankena, "Fluid Jet Polishing of optical surfaces," Appl. Opt. **37**(28), 6771–6773 (1998).
30. O. W. Faehnle, "Process optimization in optical fabrication," Opt. Eng. **55**(3), 035106 (2016).
31. L. T. Ho, C. F. Cheung, L. B. Kong, and M. J. Ren, "Theoretical and experimental investigation of three-dimensional-structured surface generation using fluid jet polishing," Proc. Institution Mechanical Eng. Part B. in press.
32. C. J. Wang, C. F. Cheung, L. T. Ho, M. Y. Liu, and W. B. Lee, "A novel multi-jet polishing process and tool for high-efficiency polishing," Int. J. Mach. Tools Manuf. **115**, 60–73 (2017).
33. C. J. Wang, C. F. Cheung, and M. Y. Liu, "Numerical modeling and experimentation of three dimensional material removal characteristics in fluid jet polishing," Int. J. Mech. Sci. under review (2017).
34. M. Y. Liu, C. F. Cheung, C. H. Cheng, R. Su, and R. K. Leach, "A Gaussian process and image registration based stitching method for high dynamic range measurement of precision surfaces," Precision Eng. 2017 (published online) https://doi.org/10.1016/j.precisioneng.2017.04.017
35. M. C. Kong, S. Anwar, J. Billingham, and D. A. Axinte, "Mathematical modelling of abrasive waterjet footprints for arbitrarily moving jets: part i – single straight paths," Int. J. Mach. Tools Manuf. **53**(1), 58–68 (2012).
36. C. Wang, W. Yang, Z. Wang, X. Yang, C. Hu, B. Zhong, Y. Guo, and Q. Xu, "Dwell-time algorithm for polishing large optics," Appl. Opt. **53**(21), 4752–4760 (2014).
37. C. Wang, Z. Wang, and Q. Xu, "Unicursal random maze tool path for computer-controlled optical surfacing," Appl. Opt. **54**(34), 10128–10136 (2015).
38. C. F. Cheung, L. B. Kong, L. T. Ho, and S. To, "Modelling and simulation of structure surface generation using computer controlled ultra-precision polishing," Precis. Eng. **35**(4), 574–590 (2011).

1. Introduction

Nowadays, optical components which possess optical microstructure array surfaces are being used in more and more products, depending on its ability to produce a unique or particular performance. These optical microstructure array surfaces are usually classified as micro-groove or channel array, micro-lens array, micro grating array, micro-pillar array, etc [1–5]. For example, micro-lens array surface have been widely used in imaging, sensing, light

Optics EXPRESS

source devices and optical interconnects [6–8]. Micro-groove array surface and other pattern surface were used to generate structure light for the measurement or imaging of complex surface [9–11].

To meet the increasing need of the optical microstructure array surfaces, many micro-machining technologies had been developed, such as micro-milling [12], chemical wet etching [13], electrical discharge machining (EDM) [14], ultra-precision diamond turning [15–17], and laser or laser assisted micro-machining [18,19]. However, these technologies either require relatively expensive equipment, or can be time-consuming. Besides, a number of other limitations also had been encountered. For example, micro-milling tool failure is difficult to predict, and tool deflection in the tool tip trajectory affects the accuracy of the desired features [20,21]. Chemical wet etching requires hazardous chemicals such as hydrogen fluoride (HF) [22]. Micro-machining with EDM suffers from electrode wear which makes it difficult to reproduce sharp corners and fillets on the workpiece. In addition, EDM can also produce large temperature variations, leading to crack formation in the workpiece [23]. Ultra-precision diamond turning can hardly be used to machine the hard materials such as glass and ceramics, and it is also difficult to be used to machine high aspect ratio microstructures. Ogura and Yoshida [24] found that micro-machining with a laser causes local melting and a heat-affected zone, which can obstruct subsequent bonding and device assembly. Though ultra-fast laser micro machining [25] can solve this problem, the machining device is too expensive. Hence, there is a need for the development of a more economic and high productivity process to fabricate the optical microstructure array surface.

Abrasive water jet machining is a cost effective way for producing micro structure array surfaces because of its ability to machine a wide range of ductile and brittle materials, with no heat affected zone and no tool wear [26,27]. Its fluid pressure could be provided at different levels so s to generate the structure surface with different aspect ratio. Haghbin et al. [28] successfully used high pressure abrasive water jet to machine micro-channels. As for the situation of low fluid pressure with pre-mixed slurry, which also called fluid jet polishing [29,30], can also be used to polish or machine three dimensional (3D)-structured surface as demonstrated by Ho et al. [31]. To enhance the polishing efficiency of fluid jet polishing, the authors [32] developed the Multi-Jet Polishing (MJP) process. However, there exists jet interference in the presented experimental results, which leads to different material removal of each jet. With this point of view, a novel fluid jet-array parallel machining (FJAPM) process is presented in this paper to implement high productivity fabrication of micro-structure array surfaces.

In the FJAPM method, an array of abrasive water jets is pumped out of a jet-array nozzle possessing a number of orifices, and each fluid jet simultaneously impinges the target surface to implement material removal independently. Moreover, the enhancement of the productivity is proportional to the number of orifices integrated in the jet array nozzle. When operated under low fluid pressure (lower than 20 bar), it could be considered as a polishing process. Moreover, it could be a micro-milling process when provides high fluid pressure (i.e. the pressure can up to thousands of bar).

In this paper, a jet array nozzle is optimally designed firstly to diminish the effect of jet interference based on the experimental investigation on the 2-Jet nozzles with different jet intervals in section 2. In section 3, the material removal characteristic was characterized and validated based on computational fluid dynamics (CFD) analysis method. Its surface generation model was also built, and several kinds of microstructure array surfaces were generated to validate this surface generation model in section 4. Following that, the effect of some factors in the process was discussed in section 5, including the fluid pressure, nozzle geometry, tool path, and dwell time.

Optics EXPRESS

2. Design of the fluid jet-array parallel machining tool

2.1 Principle of fluid jet-array parallel machining process

Figure 1 shows the principle of FJAPM process. Polishing slurry including abrasives and water are mixed adequately by mechanical stirring in a tank, and pumped at a certain pressure to a jet array nozzle as shown in Fig. 1(a). Fluid jet array with certain jet interval are generated, and impinge the target surface leading to material removal. In FJAPM, each fluid jet works independently with the same material removal characteristic, and moves along the same tool path simultaneously as shown in Figs. 1(b) and 1(c).

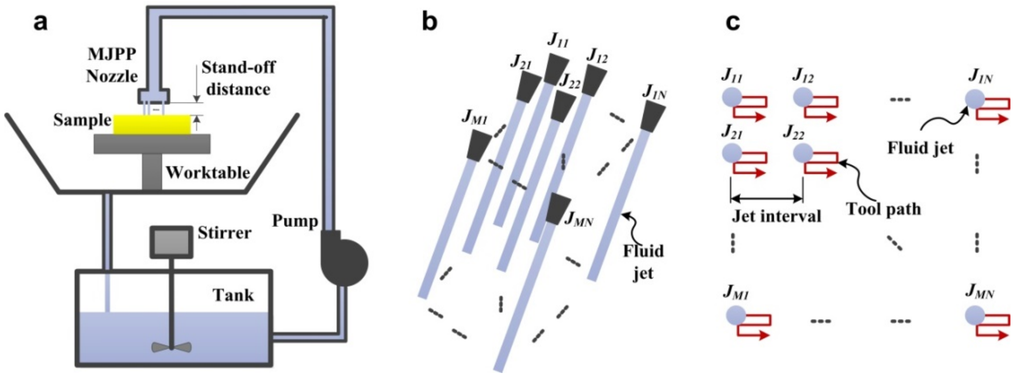

Fig. 1. Principle of Multi-Jet parallel machining process. (a) Schematic diagram of the polishing system, (b) spatial distribution of the fluid jet array, and (c) top view of synchronous movement of each fluid jet.

However, there exists jet interference which leads to the change of material removal of each fluid jet as shown in Fig. 2(a), and extra material removal at the center of the adjacent fluid jet as shown in Fig. 2(b). Hence, the jet interval must be designed large enough in FJAPM to minimize the jet interference, so as to obtain the same material removal characteristic of each fluid jet.

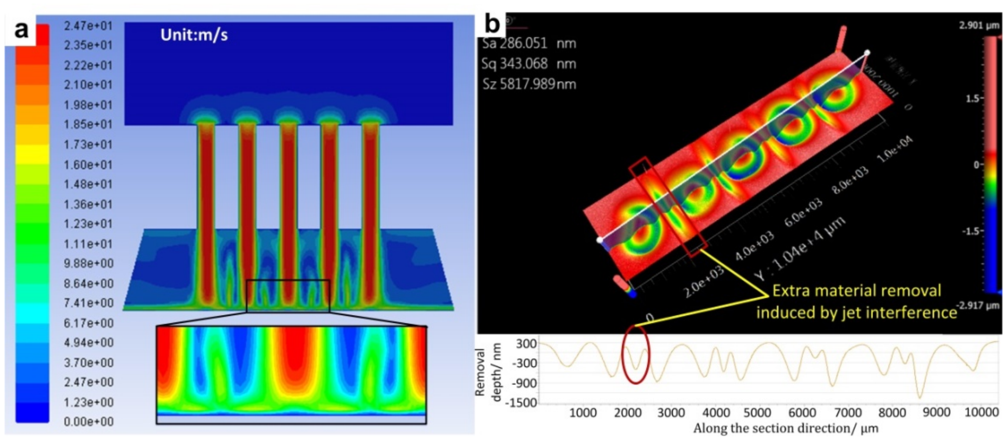

Fig. 2. Jet interference demonstration. (a) Fluid jet interference of a linear distributed 5-jet nozzle, in which the orifice diameter is 1mm and the jet interval is 2mm; (b) the corresponding material removal on BK7 with the dwell time of 3 min [32].

2.2 Optimal design of the parallel jet machining tool

To determine the suitable jet interval, a group of experiments were conducted to study the tool influence function (TIF) generation by adopting a series of 2-Jet nozzles with different jet

Optics EXPRESS

intervals. As shown in Fig. 3, the orifices of the nozzles were all designed as 0.3 mm. In this study, 440C stainless steel with heat treatment was adopted as the nozzle material. The orifices were machined through electrical discharge machining (EDM), and the practical orifice diameter was about 0.29 mm~0.34 mm. Moreover, the jet interval was designed as 0.6 mm, 1 mm, 2 mm, and 3 mm, respectively.

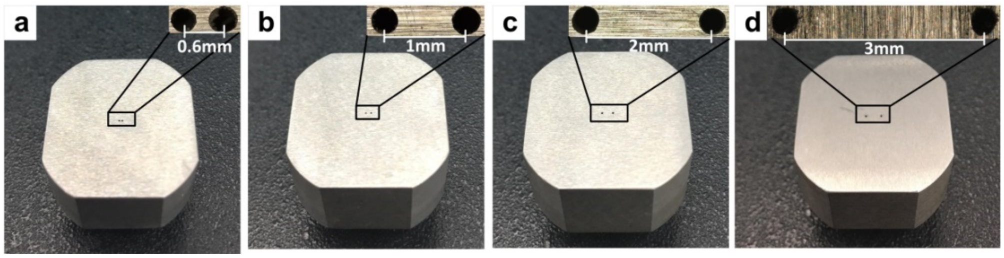

Fig. 3. Photographs of four kinds of 2-Jet nozzles with different jet interval: (a) jet interval = 0.6mm, (b) jet interval = 1 mm, (c) jet interval = 2 mm, and (d) jet interval = 3 mm.

TIF generation experiments were conducted on ZEEKO IRP200 7-axis ultra-precision polishing machine with our purposely designed nozzle. The TIF was generated on nickel copper alloys which is widely used materials for optical mold insert. 4000# silicon carbide (SiC) abrasive mixed with water was adopted as the machining slurry. Moreover, the fluid jet impinged the workpiece vertically. Table 1 summarizes the TIF generation conditions.

Table 1. TIF generation conditions

Slurry concentration	Fluid pressure (bar)	Stand-off distance[a] (mm)	Dwell time (min)
Silicon carbide: water = 1 kg:10 kg	8	3	2

[a] *The stand-off distance has been defined in Fig. 1(a).*

Figure 4 demonstrates the generated TIFs of 2-Jet nozzle with different jet interval measured by the Zygo Nexview 3D optical profilometer. As shown in Fig. 4(a), the TIF shape was distorted significantly induced by the jet interference. When the jet interval increases to 1 mm, the jet interference can still affect the TIF shape, which makes the material removal much deeper in the central region than the peripheral region as shown in Fig. 4(b). When the jet interval is 2mm, the effect of the jet interference can hardly be observed in the generated TIF as shown in Fig. 4(c), and there is no jet interference when the jet interval is 3mm as shown in Fig. 4(d). Although there are some slightly differences of each jet in Fig. 4(c) and Fig. 4(d), it may be induced by some burrs inside the orifice after EDM or the roundness of the orifice as shown from the magnified photo of the orifice in Fig. 3. Hence, when the orifice diameter is 0.3 mm, the jet interval should be larger or equal to 2 mm to minimize the effect of jet interference to the material removal. Considering that large jet interval could decrease the space utilization of the nozzle, 2mm was selected as the jet interval to design the jet array tool in this study.

Optics EXPRESS

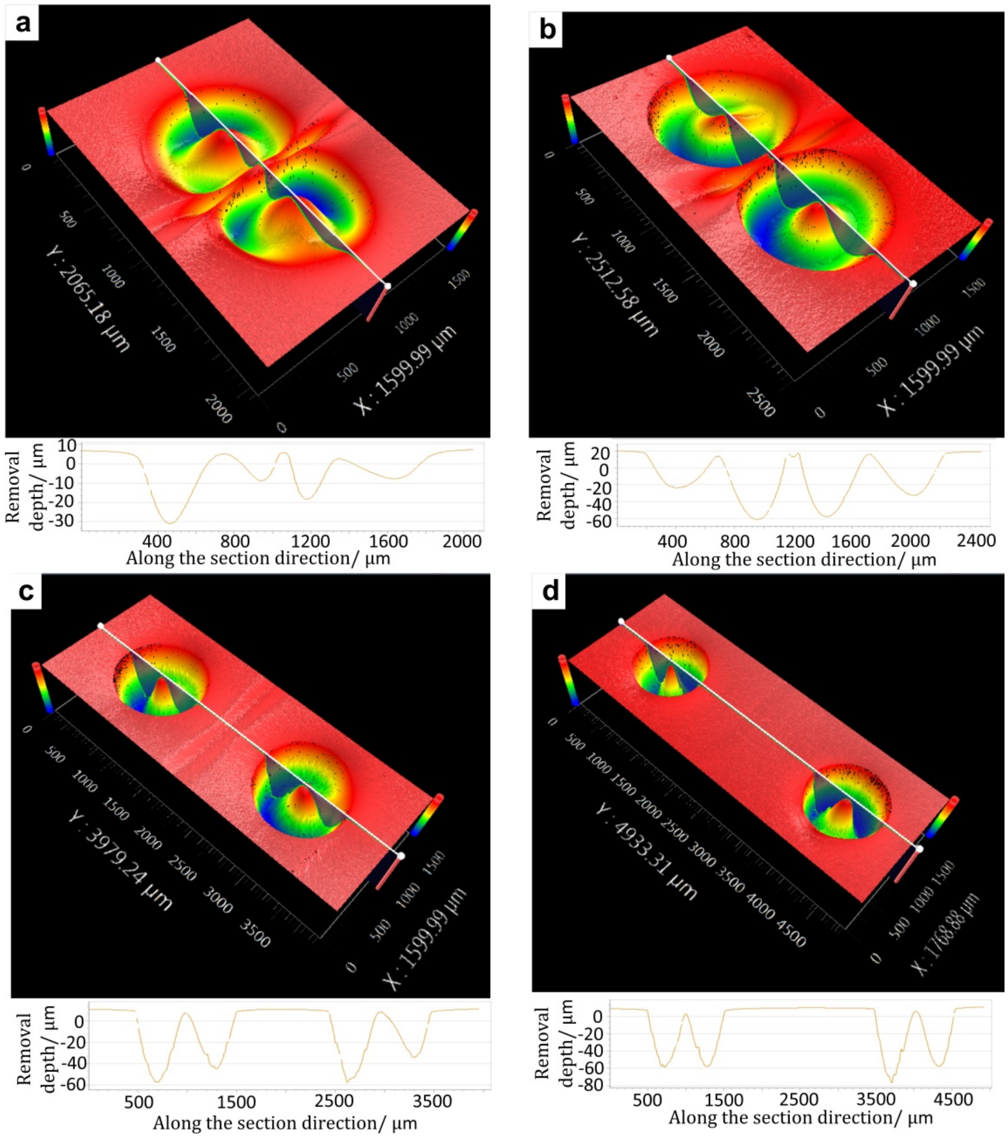

Fig. 4. Generated TIF shapes of the nozzles in Fig. 3: (a) jet interval = 0.6mm, (b) jet interval = 1mm, (c) jet interval = 2mm, and (d) jet interval = 3mm.

In this study, linear distributed 4-Jet jet array nozzle was designed as the FJAPM tool with the jet interval of 2 mm as shown in Fig. 5(a). Figure 5(b) shows its generated TIF with the same conditions as shown in Table 1. The material removal shape and the depth of each jet are very close with each other. It indicates that the jet interval of 2 mm is suitable for the FJAPM when the orifice diameter is 0.3 mm. It is interesting to noe that there exist some small differences between the TIF of each jet. These differences are mainly induced by the geometrical error of the orifice shape as shown in Fig. 5(a). Besides, the wearing of the orifice may also lead to these differences. However, it is still good enough for conducting the feasibility verification study of the fluid jet array machining method. The surface material removal after machining along a 6 mm length line with the feed rate of 0.5 mm per min was also characterized as shown in Fig. 5(c), and the shape and the form of the removed material were also closed to each other, which further validates the rationality of the jet interval of 2 mm. In order to confirm the pumped out fluid flow of each jet from the 4-jet jet array nozzle has the same fluid pressure, Computation Fluid Dynamics (CFD) simulation was conducted, and the velocity results have been shown in Figs. 5(d) and 5(e). The volume of fluid (VOF) model was employed to model the continuous multiphase, and the shear stress transport *k-ω* model was adopted to study the effect of the turbulence on the fluid flow. Other CFD model details can refer to the previous work [32] done by the authors. Moreover, the velocity of the pumped out fluid flow after 1mm distance from the nozzle was also extracted along the line shown in Fig. 5(e). It indicates that the fluid velocity of each jet is almost the same among each other, which further proves that fluid pressure of each pumped out jet is equal.

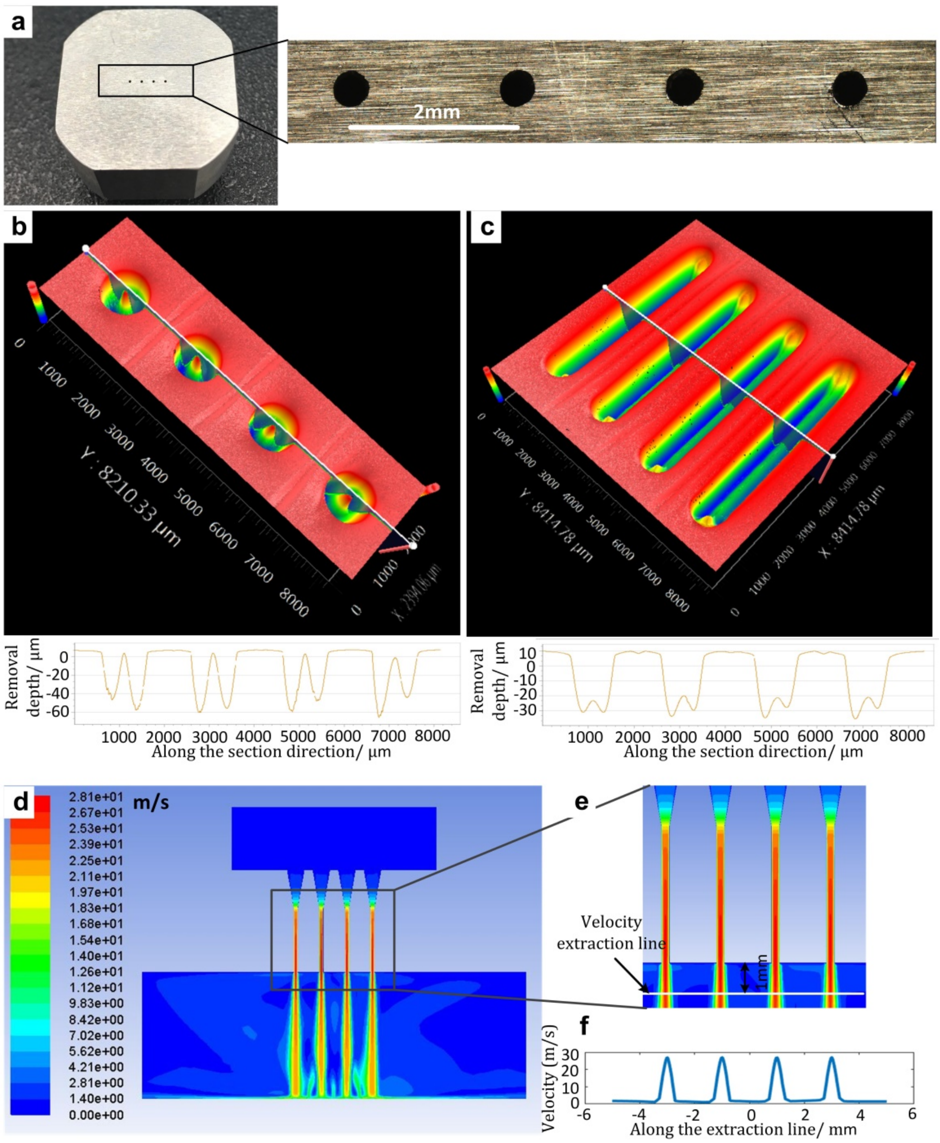

Fig. 5. Photograph and material removal characteristics of multiple linear distributed 4-jet nozzle: (a) Photograph of the multiple linear distributed 4-jet nozzle, (b) TIF contour with the dwell time of 2min, (c) generated surface form after polishing along a 6 mm length line with the feed rate of 0.5 mm/min, (d) simulated velocity distribution of the fluid flow pumped out of the 4-jet jet-array nozzle, (e) magnified figure of the region in (d), and (f) the velocity distribution of four fluid jet flow when pumped out 1mm distance.

Research Article | Vol. 25, No. 19 | 18 Sep 2017 | OPTICS EXPRESS 22717
Optics EXPRESS

3. Characterization of the material removal

As jet interference almost has no effect on the material removal of each jet, the material removal of the FJAPM can be characterized through accumulating material removal of all single jets. The maximum fluid pressure of ZEEKO IRP 200 is 20 bars. Hence, fluid jet parallel machining in this study can be treated as a polishing process. The material removal of a single jet polishing process can be characterized through combining the computational fluid dynamics analysis with a single abrasive erosion model, which can refer to the previous work by the authors [32,33] for details. The Eulerian-Lagrangian approach was used to simulate the multi-phase flow that the liquid water (continuous phase) and abrasive particles (discrete phase) are involved in. In this approach, the water and air are treated as Eulerian phase, and the abrasive particles are treated as Lagrangian phase. The Vicker's hardness of SiC is 27.445GPa in the erosion model.

Figure 6 shows the simulated results when the fluid pressure is 4 bars with the dwell time of 3 minutes, and other conditions were the same as shown in Table 1. Figure 6(a) presents the sectional fluid velocity distribution, and the material removal distribution was shown in Fig. 6(b).

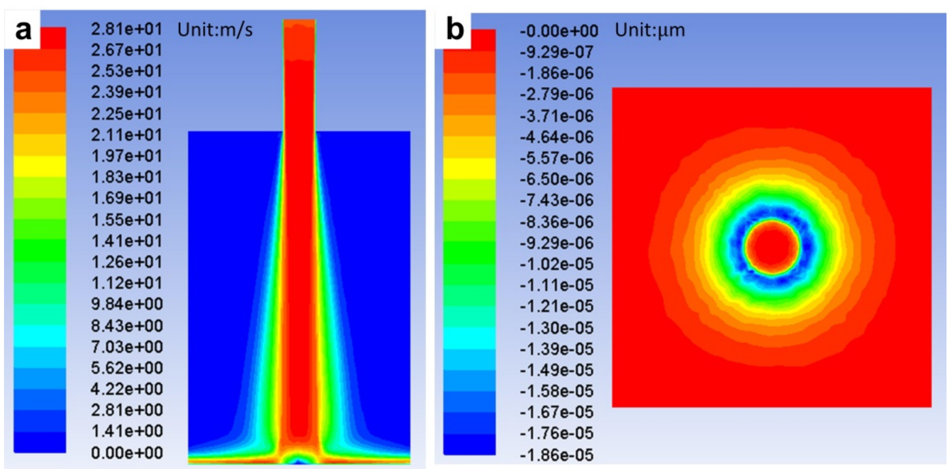

Fig. 6. Simulation results of single jet polishing when the fluid pressure is 4bar: (a) Simulated fluid velocity distribution, (b) simulated material removal distribution.

Assuming the single jet's TIF, which is the material removal depth in a unit time, can be expressed by a $K \times L$ matrix $\boldsymbol{R}_{SJ}^{[K \times L]}$. Normally, the corresponding material removal region of the TIF is smaller than the length of the jet interval. Hence, the TIF of the single jet should be extended to the size equal to the length of the jet interval, which becomes a $M \times N$ matrix $\boldsymbol{R}_{EX\_SJ}^{[M \times N]}$, where $M> = K$, $N> = L$. When $I \times J$ jet array with uniform jet interval are integrated in a jet array nozzle, its TIF $\boldsymbol{R}_{MJ}^{[P \times Q]}$ can be expressed as

$$\boldsymbol{R}_{MJ}^{[P\times Q]} = \left[\begin{array}{c} \overbrace{\hphantom{\boldsymbol{R}_{EX\_SJ}^{[(M-1)\times(N-1)]} \quad \cdots \quad \boldsymbol{R}_{EX\_SJ}^{[(M-1)\times(N-1)]} \quad \boldsymbol{R}_{EX\_SJ}^{[(M-1)\times N]}}}^{J} \\ I\left\{ \begin{matrix} \boldsymbol{R}_{EX\_SJ}^{[(M-1)\times(N-1)]} & \cdots & \boldsymbol{R}_{EX\_SJ}^{[(M-1)\times(N-1)]} & \boldsymbol{R}_{EX\_SJ}^{[(M-1)\times N]} \\ \vdots & \ddots & \vdots & \vdots \\ \boldsymbol{R}_{EX\_SJ}^{[(M-1)\times(N-1)]} & \cdots & \boldsymbol{R}_{EX\_SJ}^{[(M-1)\times(N-1)]} & \boldsymbol{R}_{EX\_SJ}^{[(M-1)\times N]} \\ \boldsymbol{R}_{EX\_SJ}^{[M\times(N-1)]} & \cdots & \boldsymbol{R}_{EX\_SJ}^{[M\times(N-1)]} & \boldsymbol{R}_{EX\_SJ}^{[M\times N]} \end{matrix} \right. \end{array} \right] \tag{1}$$

Where $P = I \times (M\text{-}1) + 1$;$Q = J \times (N\text{-}1) + 1$; $\boldsymbol{R}_{EX\_SJ}^{[(M-1) \times (N-1)]}$, $\boldsymbol{R}_{EX\_SJ}^{[(M-1) \times N]}$, $\boldsymbol{R}_{EX\_SJ}^{[M \times (N-1)]}$ are $\boldsymbol{R}_{EX\_SJ}^{[M \times N]}$ subtracted from three kinds of edges of the matrix data, respectively.

Optics EXPRESS

The TIF of the jet array nozzle can be generated through combining the simulation results of the single jet's TIF and Eq. (1). Figure 7(a) shows the measured 3D topography of the material removal distribution with the dwell time of 3 minutes, and the corresponding simulated material removal is shown in Fig. 7(b). In order to compare their shape and size accurately, the Gaussian process and image registration method was used to match the simulation and experimental results [34]. Figure 7(c) presents the matching 3D results, together with the comparison of their corresponding sectional profiles. The experimental and simulation result agrees well with each other. The deviation error was also extracted as shown in Fig. 7(d) to determine the deviation quantitatively. The root-mean-square (RMS) value of the deviation error is 1.5 μm, which is only 6.64% as compared to the maximum amplitude of the experimental data. Hence, the characterization model of the material removal characterization is effective, and can be successfully used to simulate the material removal of the FJAPM. Though some deviations can be observed in Fig. 7(c), especially the periphery part of each jet's TIF, which may be induced by the error of the model itself used in CFD or some assumptions made during the simulation process [33]. There also exist some small deviations leading to the asymmetry of the TIF, which is caused by the machined geometrical error of the orifices and the burrs inside.

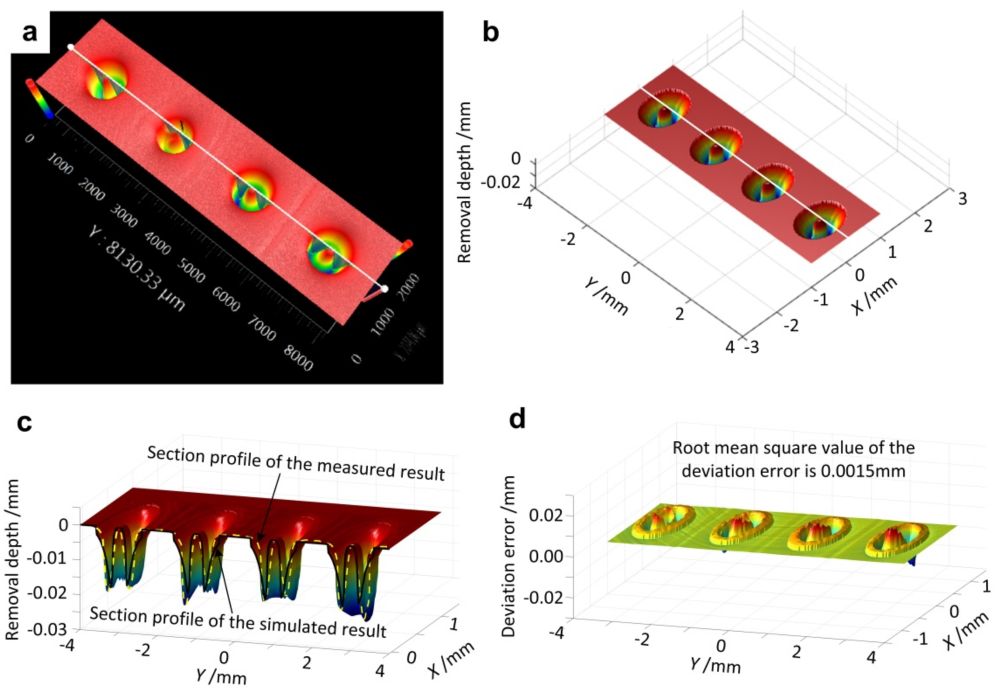

Fig. 7. Validation of the model to characterize the material removal of FJAPM: (a) measured practical material removal, (b) simulated material removal, (c) comparison of the 3D matching results marked with sectional profiles (Dash line and solid line are corresponding to the measured result and simulation result, respectively), (d) the deviation between the simulation and measured results.

4. Surface generation mechanism

4.1 Surface generation model

As for the FJAPM process utilizing low fluid pressure, the material removal is much shallower than the abrasive water jet machining process. The machined surface of the preceding step has little effect on the subsequent material removal. Hence, the material removal during the polishing process could be considered as linear material removal [35], which means that the TIF during the polishing process could be considered as the same over the whole surface. Viewing this, the surface generation of the FJAPM can still use the method adopted in deterministic polishing process [36], which are the two dimensional convolution between TIF and the dwell time. The material removal amount $\boldsymbol{H}(x,y)$ can be expressed as:

$$\boldsymbol{H}(x,y)=\boldsymbol{R}_{MJ}(x,y)*\boldsymbol{T}(x,y) \quad (2)$$

where $\boldsymbol{T}(x,y)$ is the dwell time distribution matrix. The initial surface form is assumed to be $\boldsymbol{H}_0(x,y)$, the generated surface form $\boldsymbol{E}(x,y)$ can be

$$\boldsymbol{E}(x,y)=\boldsymbol{H}_0(x,y)-\boldsymbol{H}(x,y) \quad (3)$$

In this model, the TIF matrix $\boldsymbol{R}_{MJ}$ could be the simulated one as demonstrated in section 3, and it can also be the measured result of the experimental generated TIF, which depends on the practical situation. The verification experiments of this model under these two circumstances have been presented on various microstructure array surfaces in the following part.

4.2 Model verification based on simulated tool influence function

In this section, both simulation and experiments were conducted to demonstrate the material removal along two different kinds of paths, and the simulated TIF was adopted in the simulation process. In the first kind of path, the jet array nozzle moved along an orthogonal crossed line path, and the length of each line is 6 mm. The second path is 4 sequential raster paths, and the distance between each raster path is 2 mm. Path size of each raster path is 1.6 mm × 1.6 mm with 0.1 mm scan interval. Other polishing conditions are summarized in Table 2. The workpiece is the nickel copper diamond turned flat surface, with the form error of surface smaller than 500 nm, which can reduce the effect of the initial surface error to the generated structure array surface. The polishing slurry is the same as mentioned in section 2.2. The material removal matrix as shown in Fig. 7(b) divided by 2 was taken as the TIF matrix $\boldsymbol{R}_{MJ}$. Moreover, the simulation of the surface generation was according to Eqs. (2) and (3). During the simulation of the material removal along a continuous path, the path was discretized to many high density distributed dwell points with the averaged dwell time [37].

Table 2. Polishing conditions for the validation experiments based on simulated TIF

Tool path type	Fluid pressure (bar)	Stand-off distance* (mm)	Feed rate (mm/min)
Crossed line	4	3	1
4 raster path	4	3	4

Figures 8 and 9 present the simulation and experimental results of the surface generation along these two paths, respectively. It is interesting to note that the simulated result agrees quite well with the measured result. Their deviation error between simulation and experimental results were also quantitatively determined through the matching process. The RMS values of their deviation error are only 0.31 μm and 0.61 μm. The ratio of this RMS value to the maximum amplitude of the surface form is defined as η. Hence, η of these two cases are only 5.09% and 5.93%, respectively. As shown in Figs. 8(b) and 9(b), the generated structure surface has quite good surface texture, with the arithmetic roughness (R_a) of 32 nm and 25 nm, respectively.

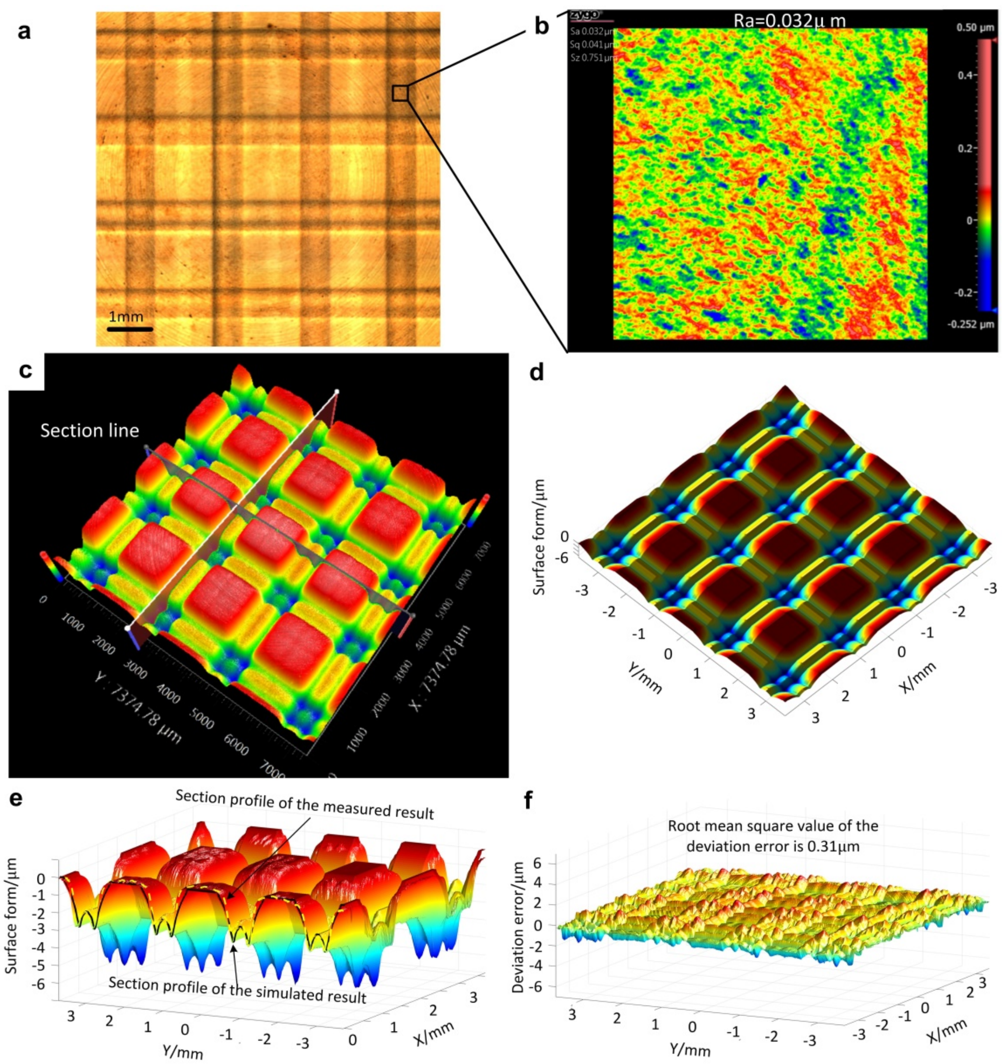

Fig. 8. Generated surface on nickel copper alloy through adopting the cross line path: (a) photo graph taken on Alicona Infinite Focus, (b) measured surface roughness of the position in (a), (c) measured surface form on Zygo Nexview 3D profilometer, and (d) simulation result of the generated surface form, (e) 3D matching results of the measured and simulated surface form, and (f) deviation error distribution.

Optics EXPRESS

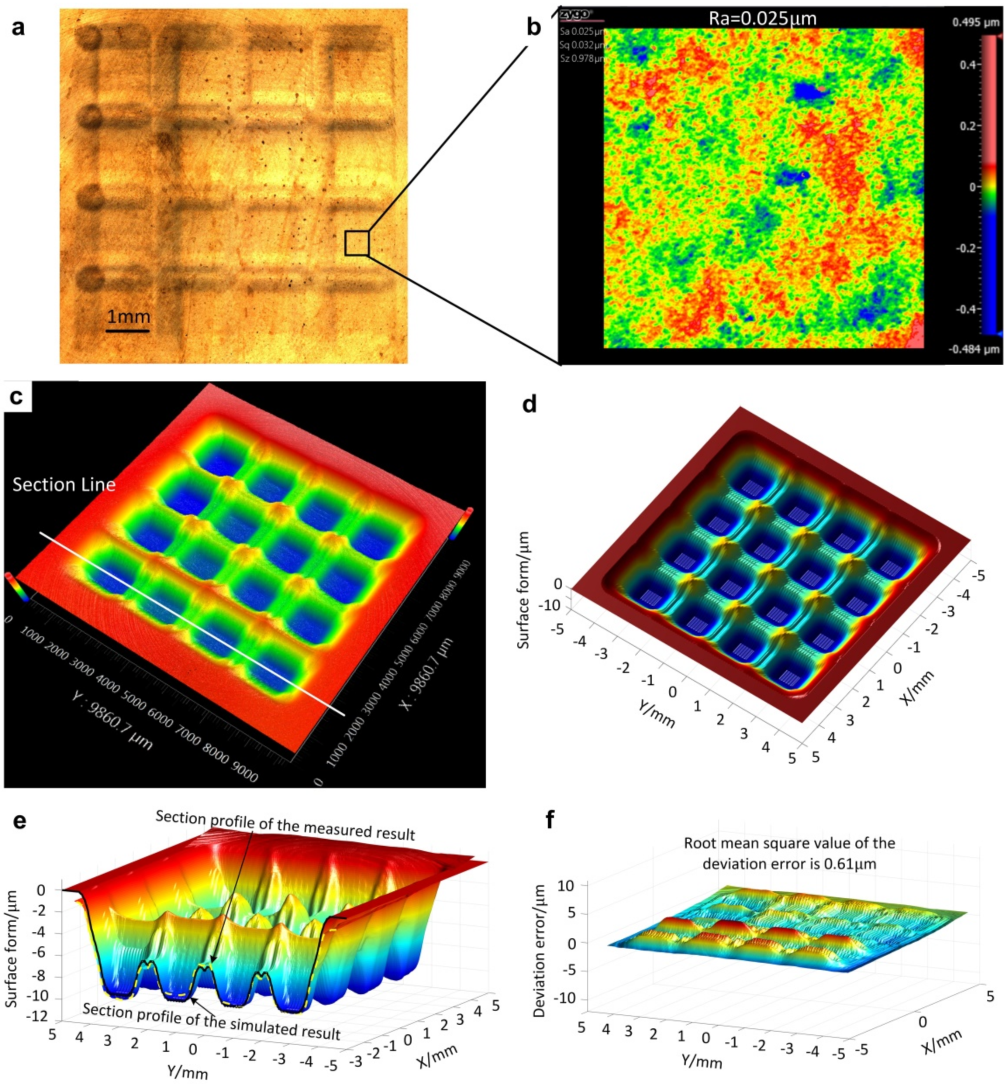

Fig. 9. Generated surface on nickel copper alloy through adopting the 4 sequential raster path: (a) photo graph taken on alicona InfiniteFocus, (b) measured surface roughness at the position shown in (a), (c) measured surface form on Zygo Nexview 3D profilometer, and (d) simulation result of the generated surface form, (e) 3D matching results of the measured and simulated surface form, and (f) deviation error distribution.

4.3 Model verification based on measured tool influence function

To further validate this surface generation model based on the measured TIFs, another two cases adopting two different paths to generate two kinds of micro-structure array surfaces were conducted in this section. The first kind of path is two adjacent 5 mm lines with the interval of 0.22 mm. Figure 5(c) has demonstrated the generated groove array when the jet array nozzle moves along one line, the deepest depth is not at the center of the groove. The deepest position of the groove can be moved to the center of the groove through the superposition of the removal of two adjacent lines. The material removal matrix as shown in Fig. 7(a) divided by 2 was taken as the TIF matrix $\boldsymbol{R_{MJ}}$, which also means that all the polishing conditions are the same with the conditions relating to the result of Fig. 7. The feed rate is 2 mm per min, and the workpiece material is nickel copper alloy. Figure 10 shows the surface generation results of this kind of groove array surface. The experimental and simulation results have reasonably with agreement with each other as shown in Fig. 10(c). The RMS of the deviation error is 0.41 μm, and η is 7.21%.

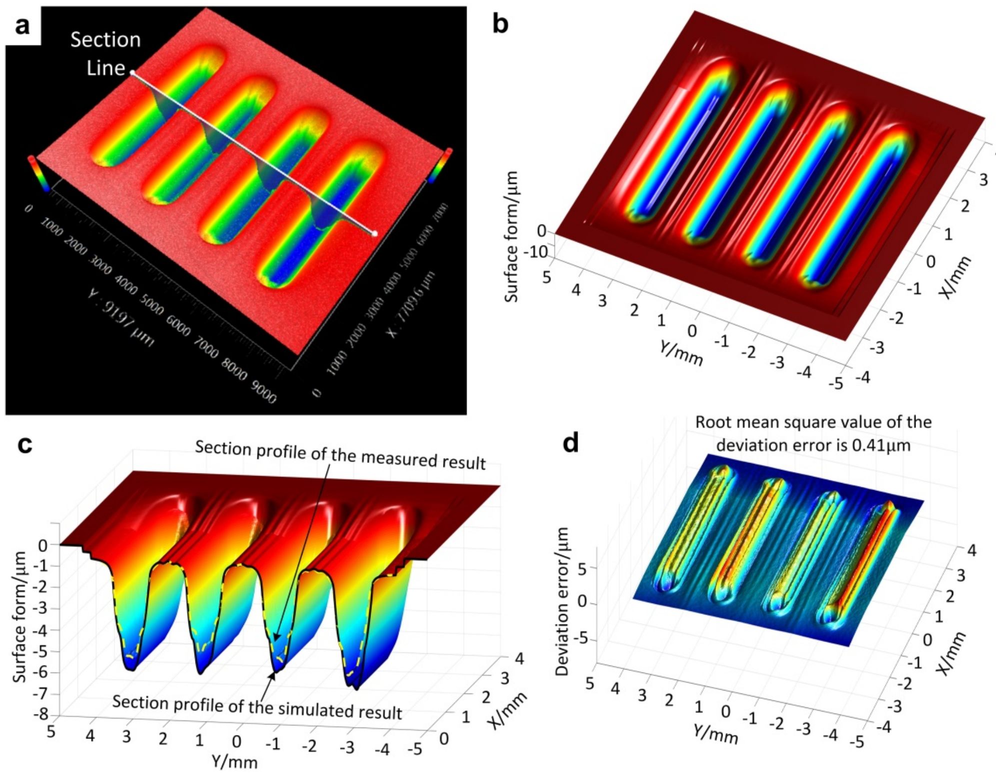

Fig. 10. Generated channel arrays with the 2-line path on nickel copper alloy: (a) measured surface form on Zygo Nexview 3D profilometer, and (b) simulation result of the generated surface form, (c) 3D matching results of the measured and simulated surface form, and (d) deviation error distribution.

The second case aims to generate a 4 × 4 lens array surface on a ground BK7 sample through adopting four sequential circle paths. The radius of each circle is 0.18 mm and the interval between each circle is 2 mm as shown in Fig. 11(a). The diameter of the BK7 sample is 20 mm. The polishing conditions are the same as mentioned in Table 2. The federate is 2 mm per minute. Each circle path was executed three times before moving to another one. The arithmetic roughness R_a of the ground BK7 surface is 0.668 μm as shown in Fig. 11(b). Moreover, the arithmetic roughness (R_a) of the generated lens array surface is 0.144 μm as shown in Fig. 11(c). Figure 11(d) shows the generated lens array surface on ground BK7 glass. The simulation of the surface generation of lens array adopting the practical TIF as showed in Fig. 11(e) was presented in Fig. 11(f). The 3D shape of them matched well with each other as shown in Fig. 11(g), and Fig. 11(h) shows the deviation error map. The RMS value of the deviation error is 0.30 μm, and η is only 3.10%. It indicates that the proposed surface generation model can be successfully used to predict the surface generation of the FJAPM process. Moreover, the maximum depth of each generated lens is compared in Fig. 11(i) to quantitatively analyze the uniformity. And the variation range is about 10.4%~8.3%. This is mainly induced by the difference of TIF of each jet as discussed in section 2.2. The non-uniformity can be minimized in a future research through adopting the ceramic or diamond nozzle material.

Optics EXPRESS

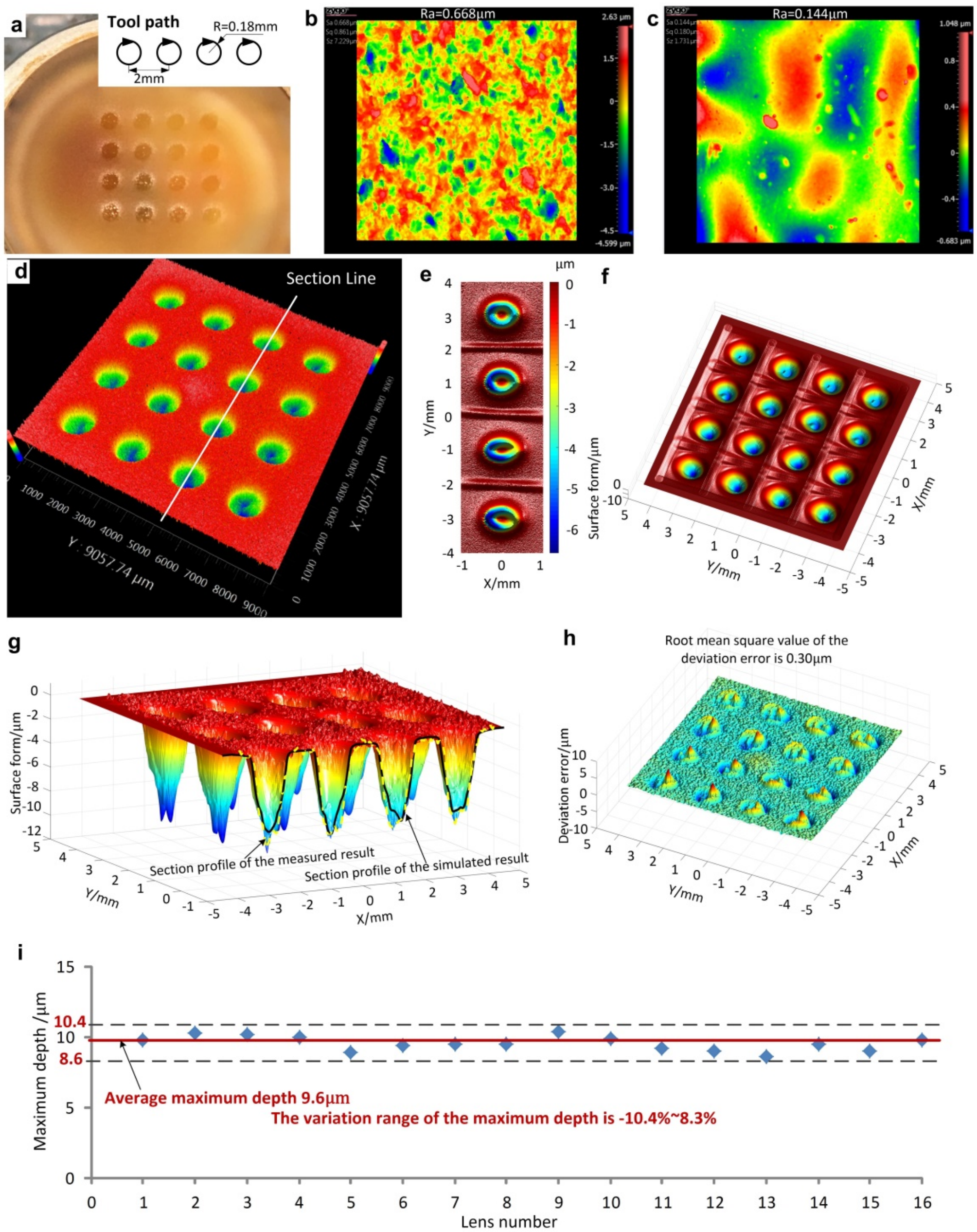

Fig. 11. Generated 4 × 4 lens array surface on ground BK7 glass: (a) photo graph of the generated lens array surface, (d) measured surface form on Zygo Nexview 3D profilometer, (e) measured practical TIF on BK7 for the simulation, (f) simulation result of the generated surface form, (g) 3D matching results of the measured and simulated surface form, (h) deviation error distribution, and (i) maximum depth comparison of the generated lens array.

The total machining time of this lens array surface is only 6 minutes 48 seconds. For classical single jet polishing, the time needs to generate for a 4 × 4 lens array would be 27 minutes 12 seconds. It infers that the utilization of the 4-jet jet array nozzle saves 3/4 of the total machining time. Moreover, the productivity of the FJAPM process can be directly proportional to the number of orifice integrated in the FJAPM nozzle. If there are 1 0 × 10 orifice designed on the FJAPM nozzle, and it is used to machine a 10 × 10 lens array surface, the total machining time would be only 1/100 of the classical single jet polishing process.

As the diameter of the orifice in the jet array nozzle in this study is 0.3 mm, the generated diameter of the lens unit is ~1.2 mm. However, the diameter of the orifice can be made as small as 10 μm. Hence, lens unit with the diameter of several tens of micrometers can also be fabricated through scaling the size of the orifice on the jet array nozzle.

5. Discussions

5.1 Effect of the fluid pressure

Limited by the experimental device used in this study, low fluid pressure (<20 bar) was provided in the above experiments. The shape of the TIF or footprint of each single jet is a ring shape, and the material removal rate is very small. Hence, the depth of the structure surface generated in this study was usually only several micrometers. Moreover, the generation of the lens array surface and micro-grooves may need a purposely designed tool path. However, when providing high fluid pressure, this process becomes a jet-array parallel milling process. The jet footprint becomes a Gaussian-like shape [27], and the shape can also be controlled through controlling its machining conditions. Under this situation, no tool path is needed to generate a lens unit for a single jet corresponding to the result in Fig. 10, and no material removal superposition is required to generate a micro-groove with the deepest depth at the center corresponding to the result in Fig. 10. With this in view, the FJAPM process could be used to generate various kinds of microstructure array surface from low aspect ratio to high aspect ratio, including the optical microstructure, through controlling the fluid pressure.

5.2 Effect of the jet array nozzle geometry

The diameter of the orifice in the study was nominally 0.3 mm, and the generated TIF size of each jet was about 1 mm. However, the size of TIF can also be controlled through adopting different sizes of the orifice. The diameter of the orifice can be made from about 10 micrometers to several millimeters. Moreover, the size of the abrasives can be tens of nanometers to several millimeters. Hence, multi-scale of the structure array surface varies from tens of micrometers to millimeters, could be fabricated through adopting the FJAPM process.

The geometrical accuracy of the orifices on the jet array nozzle, including roundness error, burrs inside, etc., is critical for the uniform material removal of each jet in the FJAPM, which can be seen from the results especially in Fig. 7. The machining error of the orifices have induced some non-uniformity of the generated structure array surface in this study, but the non-uniformity was very small which can prove that the FJAPM process is effective for machining the optical microstructure array surface. In the future, the geometrical accuracy of the orifice can be further improved through using the ceramic nozzle material and laser drilling orifice, which will improve the uniformity of the machined optical microstructure array surface.

Four orifices were integrated in the jet array nozzle in this study, which can generate four parallel fluid jets synchronously. Moreover, its productivity is four times as compared to the single jet nozzle which has been analyzed in section 4.3. When the fluid pressure can be provided large enough, tens or hundreds of orifices could be designed in one jet array nozzle. And its machining efficiency would be enhanced tens to hundreds times.

5.3 Effect of the tool path and dwell time

The FJAPM process is also a deterministic polishing process which is the same as the classical fluid jet polishing. Its material removal can also be controlled through controlling the dwell time. Cheung et al. [38] had proposed a method to generate the structure array surface through computer controlled ultra-precision polishing, and both simulation and experimental results demonstrate that it is an effective way to generate the structure array surface. With the successful fabrication of those structure arrays surfaces presented in part 4, it suggests that other structure array surfaces for different applicationd can also be fabricated by the FJAPM method through adopting different tool path plan and dwell time. With the known target structure array surface form and TIF of the FJAPM tool, the dwell time could be computed based on the dwell time calculation algorithm [35] presented before.

6. Conclusions

A novel fluid jet-array parallel machining (FJAPM) process was presented in this paper, which provides a new way to generate the microstructure array surfaces with high productivity, especially on hard and brittle materials. In this process, each pumped out fluid jet from the jet-array nozzle impinges the target surface synchronously, with almost no fluid jet interference. Hence, each jet in the FJAPM process can work independently with almost the same material removal characteristics. The material removal model and surface generation model have been built, and validated through both simulation and practical polishing experiments. The generation of several kinds of microstructure array surface utilizing the FJAPM process was also demonstrated, such as lens array surface, micro-groove array surface, etc. The results prove that the FJAPM process is an effective way to fabricate the microstructure array surface together with high productivity, whose material removal can be accurately predicted and controlled. Moreover, its machining efficiency is proportional to the number of the orifices designed in the FJAPM nozzle. Its surface generation process can be successfully predicted adopting the proposed surface generation method.

Limited by the experimental device in this study, only low fluid pressure experiments were conducted, which is fluid jet-array parallel polishing. However, it can also be extended to the machining field of high pressure fluid jet, which is fluid jet-array parallel milling. With the high fluid pressure, the form of the machined microstructure array surface would have much higher aspect ratio and material removal rate. In addition, there exists some small non-uniformity of the generated structure array surfaces, which is induced by the geometrical error of the machined orifice and wearing of the orifice. This non-uniformity could be further minimized through adopting wear-resist ceramic or diamond nozzle material in our future work.

Funding

Partner State Key Laboratories in Hong Kong from the Innovation and Technology Commission (ITC) of the Government of the Hong Kong Special Administrative Region, China; The Hong Kong Polytechnic University PhD studentship (No. RTHC) and project (No. BBX7).